ELSEVIER

Chemical Physics 206 (1996) 43–56

Chemical Physics

Theoretical study of isomeric structures and low-lying electronic states of the vinyl radical C_2H_3

Jeng-Han Wang [a], Hung-Chang Chang [a], Yit-Tsong Chen [a,b,*]

[a] *Department of Chemistry, National Taiwan University, Taipei 106, Taiwan, ROC*
[b] *Institute of Atomic and Molecular Sciences, Academia Sinica, P.O. Box 23-166, Taipei 106, Taiwan, ROC*

Received 11 November 1995

Abstract

The molecular structure, intramolecular rearrangement and dissociation energy of C_2H_3 have been studied with high-level ab initio calculations using ACES II and MOLCAS-2 programs. In the structural calculations of C_2H_3, the optimized geometry and vibrational frequencies of $\tilde{X}\ ^2A'$, the vertical electronic transition energies ($\tilde{A}\ ^2A'' \leftarrow \tilde{X}\ ^2A'$ and $\tilde{B}\ ^2A' \leftarrow \tilde{X}\ ^2A'$), the vertical ionization potential and the permanent dipole moment of $\tilde{X}\ ^2A'$ have been computed. The harmonic vibrational frequencies and infrared intensities of C_2H_3 $\tilde{X}\ ^2A'$ obtained from this calculation will help the spectroscopic observation for the vibrational modes, most of which are unobserved. The calculated vertical transition energy, 25529 cm^{-1} for $\tilde{A}\ ^2A'' \leftarrow \tilde{X}\ ^2A'$, and the vertical ionization potential, 8.33 eV from an MRCI method with atomic natural orbitals, are in excellent agreement with the experimental values of 24815 cm^{-1} and 8.25 eV, respectively. The vertical transition of $\tilde{B}\ ^2A' \leftarrow \tilde{X}\ ^2A'$, predicted to be 43910 cm^{-1} from this work, will facilitate the experimental search for the undiscovered $\tilde{B}$ state of C_2H_3 through spectroscopic observation. In calculating the intramolecular rearrangement in C_2H_3 $\tilde{X}\ ^2A'$, using CCSD(T)/Dunning's triple zeta polarizations, the non-classical structure with a hydrogen atom bridged between the C=C bond has been found to lie at least 47 kcal/mol above the classical equilibrium structure. The calculation also indicates that the non-classical C_2H_3 $\tilde{X}\ ^2A'$ is an unstable isomer, corresponding to a transition state. The computed barrier for the tunnelling of α-H in C_2H_3 $\tilde{X}\ ^2A'$ is also in excellent agreement with the upper bound limit of < 1500 cm^{-1} determined from high-resolution infrared spectroscopy. The dissociation energy of $C_2H_3 \rightarrow C_2H_2 + H$ and the energy difference between the isomers of acetylene and vinylidene, calculated in the present study, are also consistent with experimental measurements.

1. Introduction

The vinyl radical, C_2H_3, is one of the most important transient hydrocarbons in flame chemistry [1–3]. The mechanisms for the decomposition of C_2H_3, such as thermal decomposition, reactions with hydrogen [4] and oxygen [5] etc., have demonstrated to be of fundamental importance in combustion processes. It is also a significant chemical intermediate in various chemical reactions, e.g. the addition to and the polymerization of an acetylenic bond, and the decomposition of ethenoid compounds. Moreover, owing to its important role in stereochemistry, vinyl radicals have attracted the interest of organic chemists for a long time [6].

* Corresponding author. Fax: +886 2 362 0200; E-mail; ytchen@po.iams.sinica.edu.tw.

SSDI 0301-0104(95)00441-6

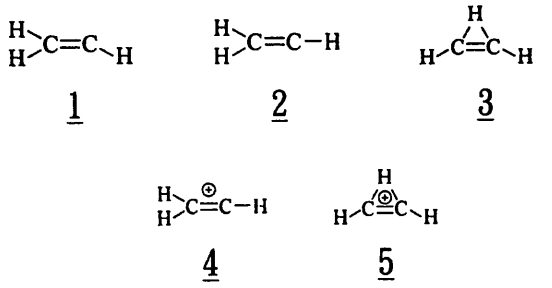

Fig. 1. The isomeric structures of vinyl radical and vinyl cation.

Geometry calculations for C_2H_3 in the ground ($\tilde{X}\,^2A'$) and the first excited ($\tilde{A}\,^2A''$) electronic states have also been the subject of many theoretical studies [7–9]. The calculated planar structures with C_S symmetry (**1** in Fig. 1) in the $\tilde{X}\,^2A'$ and the $\tilde{A}\,^2A''$ states of C_2H_3, and their associated electronic energies were used in the analysis of the low-resolution ($\Delta\nu \approx 45$ cm^{-1}) electronic $\tilde{A}\,^2A'' \leftarrow \tilde{X}\,^2A'$ absorption spectrum observed by Hunziker et al. [7]. In the observed vibrationally resolved electronic absorption spectrum of C_2H_3, the attribution for the lack of rotational features as due to the low instrumental resolution or the nature of molecular predissociation remains uncertain [7]. The ionization potential of C_2H_3 reported from several experiments [10–12], ranging from 8.95 to 8.25 eV, has also been the subject of some controversy.

Although the vibrational frequencies and dipole-moment derivatives of C_2H_3 $\tilde{X}\,^2A'$ were calculated from generalized valence bond wavefunctions many years ago [13], the ν_7 vibrational band at 895 cm^{-1} reported by Kanamori et al. [14] in gas-phase spectroscopy (~ 900 cm^{-1} in matrix isolation by Shepherd et al. [15]) has so far been the only vibrational observation. In the high-resolution infrared spectroscopy of C_2H_3, Kanamori et al. have reported the radical to be of C_{2v} effective symmetry (**2** in Fig. 1), referring to a tunnelling motion in the double-minimum potential due to the rocking α-H in C_2H_3 (as shown in Fig. 2a). The tunnelling was evidenced by (i) the spectroscopic splitting of the vibrational components in the excited $v_7 = 1$ and in the ground vibrational states, and (ii) the spectral intensity ratio of 3 : 1 for the ortho- and para-nuclear-spin statistical weights, which can only be rationalized by a C_{2v} molecular symmetry in C_2H_3 $\tilde{X}\,^2A'$. The energy barrier for the rocking motion was estimated to be < 1500 cm^{-1} from the observed spectrum [14], which is lower than the previous predictions from some relatively low-level calculations [8,13]. In this study, we have calculated the nine vibrational normal modes and infrared intensities of C_2H_3 $\tilde{X}\,^2A'$, and have tried to accurately determine the barrier of the α-H rocking motion in C_2H_3.

In contrast to the remarkable isomerization process in $C_2H_3^+$ (as shown in Fig. 2b) extensively investigated both experimentally [16] and theoretically [17], the study about the isomerization of C_2H_3 (Fig. 2c) has been relatively little reported. While the energy difference between classical (**4** in Fig. 1) and non-classical (**5** in Fig. 1) structures of $C_2H_3^+$ is only ~ 4 kcal/mol, Harding predicted the barrier for the H-migration in C_2H_3 as high as 57 kcal/mol in an earlier study [18]. In this paper, we shall report our re-examination of the energy difference between the classical (**1** in Fig. 1) and non-classical (**3** in Fig. 1) structures of C_2H_3 with high-level ab initio calculations. The very recent calculation of the methylcarbyne–vinyl isomerization conducted by Nielsen et al. is worth noticing [19]. The calculated isomerization barrier and energy difference from methylcarbyne to vinyl radical are 9 and −49 kcal/mol, respectively, in the doublet potential, and 57 and −3 kcal/mol in the quartet. The calculations have signified that the spectroscopic observation from vinyl to methylcarbyne is much more difficult than the reversed isomerization process.

Of particular interest to us with the vinyl radical

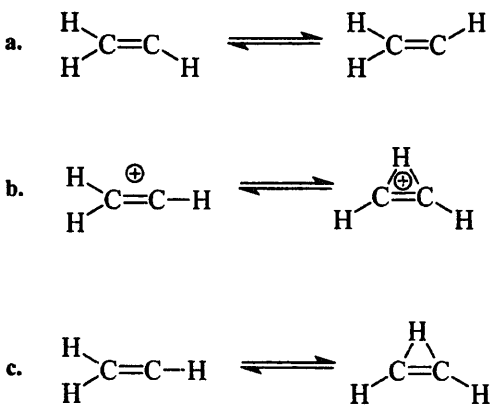

Fig. 2. The intramolecular rearrangements in vinyl radical and vinyl cation.

is to experimentally investigate the *isomerization* and the *dissociation* processes of C_2H_3 $\tilde{X}\,^2A'$ in our laboratory by vibration-rotationally state-selective laser spectroscopy, such as stimulated emission pumping (SEP) [20] or two-color (IR-UV) laser-induced grating (LIG) [21]. To facilitate the experimental performance in the SEP and LIG spectroscopies, we have calculated the vertical electronic transition frequencies. Owing to the likely predissociation in the first excited electronic state ($\tilde{A}\,^2A''$) of C_2H_3 as discussed by Hunziker et al. [7], we have sought an alternative and calculated the second excited electronic state of the radical. We have also calculated the vertical ionization potential of C_2H_3 to compare with the experimental result [12] to test the accuracy of the computational process. In this paper, we shall also report the calculations of the energy required for the C–H bond cleavage in the dissociation of $C_2H_3 \rightarrow H + HCCH$ (acetylene) or $C_2H_3 \rightarrow H + H_2CC$ (vinylidene). The calculated results will show that the isomerizations are energetically above the dissociation threshold of $C_2H_3 \rightarrow H + HCCH$.

This paper is organized as follows. In Section 2, we will describe the computational details for the calculations of the *molecular structure, intramolecular rearrangement* and *dissociation* of C_2H_3 using ACES II [22] and MOLCAS-2 [23] programs. For the *molecular structure* of C_2H_3, we have calculated (i) the equilibrium geometry and vibrations of the ground electronic state ($\tilde{X}\,^2A'$), (ii) the isomeric structures on the ground electronic potential, (iii) the vertical transitions from the ground ($\tilde{X}\,^2A'$) to the first ($\tilde{A}\,^2A''$), and to the second ($\tilde{B}\,^2A'$) excited electronic states, respectively, (iv) the vertical ionization potential, and (v) the permanent dipole moment of $\tilde{X}\,^2A'$. Calculations of the *intramolecular rearrangement* in C_2H_3 include isomerization and α-H rocking motion as shown in Fig. 2. In the study of the *dissociation* in C_2H_3 $\tilde{X}\,^2A'$, we have calculated the dissociation energies of $C_2H_3 \rightarrow H + HCCH$, and of $C_2H_3 \rightarrow H + H_2CC$. The energy difference between the isomers of acetylene and vinylidene has also been computed. In Section 3, we will discuss the calculated results obtained in the present study using high-level ab initio methods with various efficient basis sets. Concluding remarks will be addressed in Section 4.

2. Computational details

All of the calculations carried out in this study were executed on an IBM RISC6000/590 computer. The computational schemes for molecular structure, intramolecular rearrangement and dissociation of C_2H_3 using the programs of ACES II and MOLCAS-2 will be described in the following.

2.1. Molecular structure

2.1.1. Equilibrium geometry and vibrations of C_2H_3 $\tilde{X}\,^2A'$

Using the ACES II program, we have optimized the ground electronic structure of C_2H_3. The ab initio methods, including many body perturbation theory (MBPT) and coupled cluster (CC), have been employed in the *full optimization for the nine internal co-ordinates* in C_2H_3. The basis sets for the carbon and hydrogen atoms of C_2H_3 were 6-31G** and Dunning's DZP, TZP, TZ2P and PVTZ. In the optimization, UHF MOs were used as approximate starting wavefunctions, and the vinyl radical was set to be of C_1 symmetry. The labelling for each atom in the equilibrium structure of C_2H_3 is shown in Fig. 3. The completion of the optimization was reached at an energy gradient of $\leqslant 1 \times 10^{-4}$ hartree/bohr. The optimized geometry of the ground electronic state of C_2H_3, using various methods and basis sets, together with the calculated rotational constants are listed in Table 1. Since the dihedral angles in the optimized geometry of the ground electronic state of C_2H_3 are very small ($\leqslant 0.02°$ in all of the calculations) and are not shown in Table 1, the structure is essentially planar. The symmetry of the ground electronic state of C_2H_3 is therefore an A′ representation belonging to the C_S molecular symmetry group, i.e. $\tilde{X}\,^2A'$.

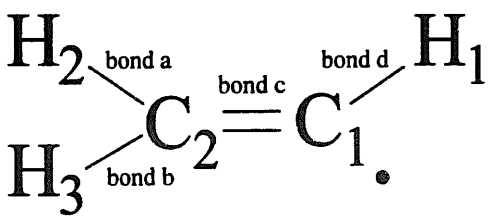

Fig. 3. The labelling for each atom in classical C_2H_3. The core electrons ($1s^2$) of the carbon are not shown.

Table 1
The optimized geometry, rotational constants and fundamental vibrations of classical C_2H_3 $\tilde{X}\,^2A'$ [a]

Method Basis	Exp. [b]	GVB [c] 6-31G**	SCF [d] TZ2P	MP2 DZP	MP2 TZ2P	MP4 DZP	CCSD(T) 6-31G**	CCSD(T) DZP	CCSD(T) TZP	CCSD(T) C:PVTZ, H:DZP	CCSD(T) TZ2P
equilibrium geometry [e]											
$r_{C_1H_1}$	1.080±0.010	1.085	1.069	1.128	1.074	1.132	1.079	1.090	1.082	1.082	1.078
$r_{C_1C_2}$	1.3160±0.0063	1.332	1.299	1.380	1.281	1.381	1.321	1.334	1.320	1.306	1.314
$r_{C_2H_2}$	1.085±0.010	1.095	1.077	1.111	1.084	1.112	1.089	1.098	1.088	1.089	1.088
$r_{C_2H_3}$	1.085±0.010	1.093	1.074	1.105	1.080	1.107	1.084	1.093	1.093	1.094	1.083
$\angle C_2C_1H_1$	137.3±4.0	134.2	135.03	105.5	137.4	105.5	135.7	135.0	136.8	137.6	136.6
$\angle C_1C_2H_2$	121.5±1.0	121.5	121.17	127.5	121.0	127.4	121.7	121.2	121.2	122.0	121.2
$\angle H_3C_2H_2$	117.0±1.4	117.3	117.21	111.7	116.8	111.7	116.3	117.0	117.0	116.5	116.7
rotational constants											
A	7.90934			6.14587	7.90496	6.12142	7.75286	7.53288	7.75403	7.80020	7.80069
B	1.083026			1.06165	1.13182	1.05862	1.07662	1.05873	1.07430	1.09104	1.08499
C	0.948643			0.90527	0.99006	0.90254	0.94534	0.92826	0.94357	0.95716	0.95250
fundamental vibrations [f]											
ν_1		3265	3391	3144	3321	3115	3308	3261	3261	3241	3215
				(9.7646)	(2.4961)	(14.2606)	(2.5145)	(1.0708)	(1.2979)	(1.3074)	(1.0471)
ν_2		3192	3352	3056	3264	3036	3251	3227	3199	3162	3156
				(1.4000)	(0.1130)	(0.8738)	(8.2941)	(6.2158)	(1.1556)	(1.0543)	(1.0733)
ν_3		3116	3266	2929	3157	2880	3144	3113	3090	3062	3049
				(11.3414)	(0.1583)	(13.0099)	(5.7128)	(3.7732)	(1.0299)	(1.2277)	(1.0007)
ν_4		1670	1774	1537	1895	1527	1664	1619	1630	1661	1609
				(9.9257)	(5.9740)	(8.5723)	(0.8039)	(1.8930)	(2.5655)	(2.1153)	(3.2147)
ν_5		1444	1513	1303	1443	1290	1436	1401	1402	1395	1411
				(12.1168)	(12.0570)	(11.6282)	(3.6553)	(4.6947)	(6.5126)	(7.7336)	(6.3769)
ν_6		1185	1204	1197	1104	1238	1108	1095	1074	1060	1098
				(0.7185)	(8.0583)	(0.3519)	(8.2656)	(6.2536)	(6.2758)	(7.2704)	(6.6299)
ν_7	895.1624	918	1054	1091	1059	1070	929	895	917	927	944
				(82.5193)	(80.8138)	(78.2787)	(66.4135)	(78.7289)	(83.3655)	(71.6973)	(74.9015)
ν_8		827	959	913	978	899	818	763	807	830	830
				(2.1864)	(26.9113)	(2.0558)	(2.7927)	(0.5581)	(5.0018)	(10.9344)	(9.7368)
ν_9		783	830	913	750	881	763	746	730	714	764
				(14.1836)	(18.9848)	(12.7251)	(15.8375)	(14.7487)	(18.4564)	(19.0132)	(17.2525)
energy		−77.465265		−77.63680	−77.71697	−77.67682	−77.68323	−77.71302	−77.74103	−77.77343	−77.76493
zero-point energy				22.993	24.261	22.783	23.474	23.042	23.032	22.948	22.980

[a] ACES II was used in the calculation. Bond lengths in Å, bond angles and dihedral angles in deg, rotational constants in cm^{-1}, vibrational frequencies in cm^{-1}, energy in au, and zero-point energy in kcal/mol.
[b] Ref. [14].
[c] Ref. [13].
[d] Ref. [19].
[e] The dihedral angles in the optimized geometry are very small ($\leq 0.02°$ in all of the calculations) and are not listed. The structure of C_2H_3 is essentially planar.
[f] The numbers in parentheses are the infrared intensities in km/mol.

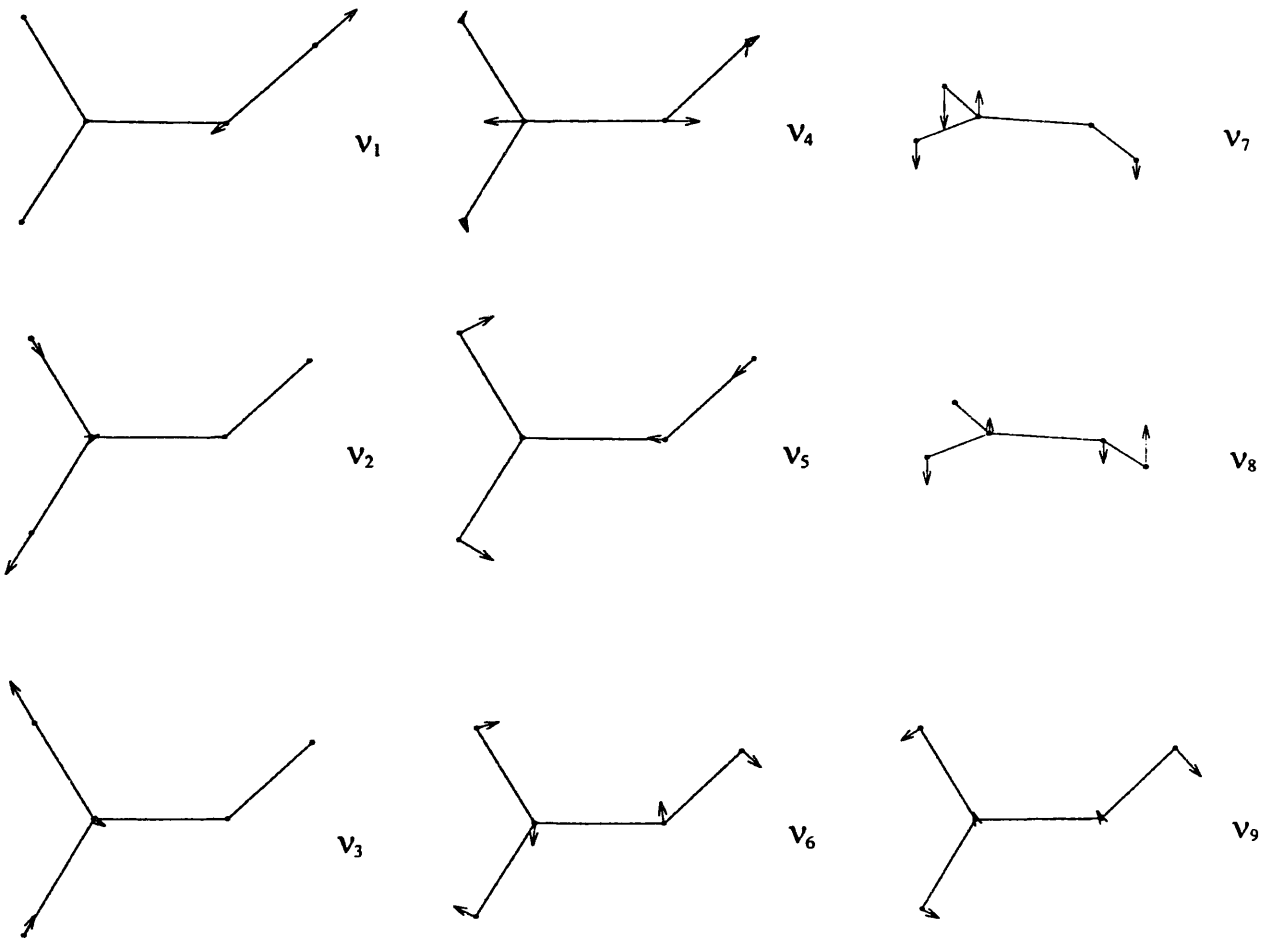

Fig. 4. The vibrational normal modes of classical C_2H_3 $\tilde{X}\,^2A'$.

After completing the optimization, we proceeded to calculate the fundamental vibrational frequencies of C_2H_3 $\tilde{X}\,^2A'$ by diagonalizing the force-constant matrix and transforming the dipole-moment gradient to normal co-ordinates. The calculated fundamental vibrational frequencies of C_2H_3 $\tilde{X}\,^2A'$ are also tabulated in Table 1. The nine vibrational normal modes are shown in Fig. 4.

2.1.2. *Electronic energies, ionization potential and dipole moment*

In the MOLCAS calculations of C_2H_3, the methods from RASSCF to MRCI have been applied to compute the vertical transitions from the ground to the first, and to the second excited electronic states. The vertical ionization potential and permanent dipole moment of C_2H_3 $\tilde{X}\,^2A'$ have also been included in the calculation. The generally contracted basis sets of atomic natural orbital (ANO) [24] have been used in the present study. At the beginning, smaller basis sets of the ANO-type contractions were used, such as [4s3p2d] for the carbon and [2s1p] for the hydrogen of C_2H_3 composed of the primitive sets of (14s9p4d) and (8s4p), respectively. More complete basis sets of ANO contractions, [4s3p2d1f] from primitive

Table 2
The selected frozen orbitals in the MOLCAS calculation [a]

Number of frozen orbitals	Frozen orbitals
2	cores a and b
3	cores a and b; bond c (σ)
4	cores a and b; bonds a and b
5	cores a and b; bonds a, b and c (σ)
6	cores a and b; bonds a, b and c ($\sigma + \pi$)

[a] Cores a and b are 1s electrons of C_1 and C_2.

Table 3
The vertical electronic transition energy, ionization potential, and the permanent dipole moment of classical C_2H_3 $\tilde{X}^2A'$

Method	Exp.	Previous works	RASSCF	RASSCF	RASSCF	RASSCF	RASSCF	RASSCF	MRCI
Basis for C			4s3p2d	4s3p2d1f	4s3p2d	4s3p2d	4s3p2d	4s3p2d	4s3p2d1f
Basis for H			2s1p	3s2p1d	2s1p	2s1p	2s1p	2s1p	3s2p1d
Frozen orbitals			5	5	4	4	6	3	5
Active orbitals [a]			5 (3H,2L)	5 (3H,2L)	7 (4H,3L)	6 (4H,2L)	5 (2H,3L)	7 (5H,2L)	5 (3H,2L)
vertical transition energy [b]									
$\tilde{X}^2A' \rightarrow \tilde{A}^2A''$ (cm^{-1})	24815 [c]	26100 [c]	28359	28299	28076	27955	25233	27626	25529
$\tilde{X}^2A' \rightarrow \tilde{B}^2A'$ (cm^{-1})			50969	43279	44451	43783	43018	43545	43910
$\tilde{X}^2A' \rightarrow C_2H_3^+ + e^-$ (eV)	$8.25^{-0.05}_{+0.20}$ [d] 8.59 ± 0.03 [f] 8.95 [g]	8.64 [e]	8.73	8.71	8.73	8.62	9.42	8.47	8.33
dipole moment (D)		0.576 [h]	0.563	0.563	0.460	0.545	0.588	0.563	
ground electronic energy (a.u.)		−77.6922 [i]	−77.44873	−77.45239	−77.46712	−77.45392	−77.44094	−77.45839	−77.45239

[a] (mH, nL) represents the m highest HOMOs and the n lowest LUMOs used in the MOLCAS calculation.
[b] $C_2H_3^+$ is in the singlet classical structure.
[c] From Ref. [7].
[d] From Ref. [12].
[e] From Ref. [9].
[f] From Ref. [11].
[g] From Ref. [10].
[h] From Ref. [13], GVB/6-31G**.
[i] From Ref. [9], MP4/6-311G**.

(14s9p4d3f) for the carbon and [3s2p1d] from (8s4p3d) for the hydrogen, have been employed later in the calculation. The sizes of the contracted basis sets for the smaller and for the more complete ones are 51 and 102, respectively.

Since the geometry optimization can not be carried out in the MOLCAS-2 program, the optimized equilibrium geometry of C_2H_3 $\tilde{X}\,^2A'$, obtained from the ACES II calculation using CCSD(T) and PVTZ/DZP, has been transferred into the MOLCAS computation to calculate the vertical transitions from the ground ($\tilde{X}$) to the first excited ($\tilde{A}$), and to the second excited ($\tilde{B}$) electronic states of C_2H_3. We have tested various sets of frozen and active orbitals in the MOLCAS calculation. The selected frozen orbitals in different approaches are listed in Table 2 and the corresponding labelling for the chemical bonds in C_2H_3 is shown in Fig. 3. We have taken the high occupied and the low virtual molecular orbitals of C_2H_3, shown in Table 3, as a restricted active space (RAS). From the occupied molecular orbitals, the electronic configurations for the $\tilde{X}$, $\tilde{A}$, and $\tilde{B}$ states of C_2H_3 are $(1a')^2(2a')^2(3a')^2(4a')^2(5a')^2(6a')^2(1a'')^2(7a')^1$, $(1a')^2(2a')^2(3a')^2(4a')^2(5a')^2(6a')^2(1a'')^1(7a')^2$, and $(1a')^2(2a')^2(3a')^2(4a')^2(5a')^2(6a')^2(1a'')^1(7a')^1(2a'')^1$, respectively, where the 1a'', 7a' and 2a'' molecular orbitals have, in turn, been characterized by π-bonding, σ-bonding (occupied by the single electron on C_1 in Fig. 3), and π^*-bonding. From the electronic configurations, we have been able to identify the symmetry of the ground, the first and the second excited electronic states of C_2H_3 (in terms of a C_S molecular symmetry group) as $\tilde{X}\,^2A'$, $\tilde{A}\,^2A''$ and $\tilde{B}\,^2A'$, respectively.

The reference configurations for the $\tilde{X}\,^2A'$, $\tilde{A}\,^2A''$, $\tilde{B}\,^2A'$ electronic states of C_2H_3, and the vinyl cation used in the calculations are listed in Table 4. The resulted vertical transition energies, ionization potential and permanent dipole moment from the RASSCF calculations are tabulated in Table 3. After using the GUGA selection reference, we have tried an MRCI method with the basis sets of ANO contractions, [4s3p2d1f] for the carbon and [3s2p1d] for the hydrogen, to calculate the vertical electronic transitions of $\tilde{A}\,^2A'' \leftarrow \tilde{X}\,^2A'$ and $\tilde{B}\,^2A' \leftarrow \tilde{X}\,^2A'$ and the vertical ionization potential of C_2H_3. In the GUGA selection, five frozen and five active orbitals have been chosen. For the active orbitals, three HOMO, and two LUMO, were involved in the calculation. The MRCI results are listed in Table 3. In comparison with the experimental values for the vertical transition in $\tilde{A}\,^2A'' \leftarrow \tilde{X}\,^2A'$ and the vertical ionization potential of C_2H_3, the accuracy of the computational procedures in the present calculation has been tested, and will be discussed in Section 3.

2.2. Intramolecular rearrangement

2.2.1. Isomerization

In the study of the hydrogen-migration in C_2H_3 $\tilde{X}\,^2A'$, the energy difference between the classical (**1** in Fig. 1) and the non-classical (**3** in Fig. 1) isomers has been calculated exclusively with the ACES II program. At the beginning of the optimization for the non-classical C_2H_3, we tried a full optimization

Table 4
The reference configurations for the $\tilde{X}\,^2A'$, $\tilde{A}\,^2A''$ and $\tilde{B}\,^2A'$ electronic states of C_2H_3 and the vinyl cation [a]

Electronic state	Reference configuration				
ground ($\tilde{X}\,^2A'$)	22100 (0.9604)	20120 (0.0351)	21110 (0.0062)	02102 (0.0033)	
the first excited ($\tilde{A}\,^2A''$)	21200 (0.8848)	21110 (0.0567)	21020 (0.0483)	20210 (0.0058)	12200 (0.0039)
the second excited ($\tilde{B}\,^2A'$)	21110 (0.9754)	12200 (0.0977)	11210 (0.0074)	22100 (0.0073)	21011 (0.0040)
vinyl cation ($C_2H_3^+$) [b]	22000 (0.9456)	20020 (0.0310)	11110 (0.0101)	02200 (0.0040)	02002 (0.0032)

[a] The number in parentheses represents a weight for the configuration used in the MRCI calculation.
[b] $C_2H_3^+$ is in the singlet classical structure.

Table 5
The optimized geometry, rotational constants and fundamental vibrations of non-classical C_2H_3 $\tilde{X}\,^2A'$ [a]

Method Basis	SCF DZP	SCF TZP	SCF TZ2P	SOGVB [b] DZP	MP2 DZP	MP2 TZ2P	MP4 DZP	CCSD(T) 6-31G**	CCSD(T) DZP	CCSD(T) TZP	CCSD(T) C:PVTZ, H:DZP	CCSD(T) TZ2P
Equilibrium geometry [c]												
$r_{C_1H_1}$	1.289	1.283	1.282	1.275	1.279	1.267	1.290	1.282	1.299	1.290	1.288	1.287
$r_{C_2H_1}$	1.289	1.283	1.282									
$r_{C_1H_2}$	1.081	1.077	1.074	1.094	1.082	1.097	1.087	1.098	1.090	1.090	1.085	
$r_{C_2H_3}$	1.081	1.077	1.074									
$r_{C_1C_2}$	1.287	1.277	1.272	1.290	1.314	1.294	1.317	1.305	1.317	1.306	1.292	1.299
$\angle H_3C_2H_1$	153.5	153.1	153.2	154.4	153.5	153.2	153.7	154.4	154.0	153.6	153.3	153.7
$\angle H_2C_1H_1$	153.5	153.1	153.2									
$\langle^{H_3C_2H_1}_{H_1C_1C_2}$	180.0	180.0	180.0	180.0	179.8	179.3	180.0	180.0	180.0	180.0	180.0	
$\langle^{H_2C_1H_1}_{H_1C_1C_2}$	180.0	180.0	180.0									
rotational constants												
A					8.79705	8.97430	8.61205	8.57955	8.41586	8.58413	8.55595	8.58991
B					1.09729	1.12876	1.09149	1.11708	1.09334	1.11285	1.12988	1.12446
C					0.97560	1.00265	0.96872	0.98839	0.96763	0.98514	0.99808	0.99430
fundamental vibrations [d]												
ν_1					3220 (B)	3197 (A)	3157 (B)	3184 (A)	3148 (A)	3152 (A)	3135 (A)	3144 (A)
ν_2					3198 (A)	3156 (B)	3154 (A)	3140 (B)	3099 (B)	3105 (B)	3088 (B)	3099 (B)
ν_3					2800 (B)	2535 (A)	2589 (B)	2420 (A)	2414 (A)	2388 (A)	2392 (A)	2357 (A)
ν_4					2575 (A)	1717 (A)	2494 (A)	1745 (A)	1715 (A)	1707 (A)	1734 (A)	1700 (A)
ν_5					1706 (A)	918 (A)	1687 (A)	935 (A)	894 (A)	917 (A)	899 (A)	907 (A)
ν_6					907 (A)	829 (B)	902 (A)	858 (B)	807 (B)	831 (B)	819 (B)	824 (B)
ν_7					803 (B)	701 (A)	794 (B)	708 (A)	661 (A)	715 (A)	775 (A)	686 (A)
ν_8					681 (A)	232 (B)	654 (A)	159 (B)	101 (B)	236 (B)	289 (B)	103 (B)
ν_9					219 (B)	55i (B)	148 (B)	2158i (B)	2143i (B)	2123i (B)	2115i (B)	2140i (B)
energy				−77.33942	−77.58874	−77.64215	−77.62435	−77.59489	−77.62692	−77.65716	−77.69237	−77.68075
zero-point energy					23.027	18.993	22.271	18.796	18.210	18.657	18.772	18.328

[a] ACES II was used in the calculation. Bond lengths in Å, bond angles and dihedral angles in deg, rotational constants in cm^{-1}, vibrational frequencies in cm^{-1}, energy in au, and zero-point energy in kcal/mol.
[b] From Ref. [9].
[c] $\langle^{H_3C_2H_1}_{H_1C_1C_2}$ and $\langle^{H_2C_1H_1}_{H_1C_1C_2}$ represent the dihedral angles.
[d] The A/B in parentheses is the symmetry representation of a C_2 molecular symmetry group.

Table 6
The energy difference between the classical and non-classical C_2H_3 $\tilde{X}^2A'$

Method	SOGVB [a]	POL-CI [a]	POL-CI(S + D) [a]	MP2	MP2	MP4	CCSD(T)	CCSD(T)	CCSD(T)	CCSD(T)	CCSD(T)
Basis	DZP	DZP	DZP	DZP	TZ2P	DZP	6-31G**	DZP	TZP	C:PVTZ, H:DZP	TZ2P
classical (au)				−77.63680	−77.71697	−77.67682	−77.68323	−77.71302	−77.74103	−77.77343	−77.76493
non-classical (au)	−77.33942	−77.441984	−77.4521	−77.58874	−77.64215	−77.62435	−77.59489	−77.62692	−77.65719	−77.69237	−77.68075
energy difference [b]	22839	19411	19936	10548	16421	11516	19388	18897	18407	17791	18475
(cm^{-1})				(10560)	(14578)	(11337)	(17752)	(17524)	(16877)	(16330)	(16848)

[a] From Ref. [18].

[b] The number in parentheses represents the zero-point energy corrections for both classical and non-classical C_2H_3.

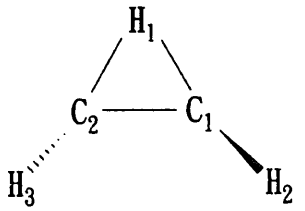

Fig. 5. The atomic labelling of non-classical C_2H_3 $\tilde{X}\,^2A'$.

process (including nine internal co-ordinates) using an SCF method and the Dunning basis sets of DZP, TZP and TZ2P. The optimized results are listed in Table 5 and the corresponding atomic labelling is shown in Fig. 5. The optimized non-classical C_2H_3 is essentially planar and possessed of C_{2v} symmetry. In the later calculations with higher-level methods,

Table 7
The optimized geometry, rotational constants, and fundamental vibrations of the transition state of C_2H_3 $\tilde{X}^2A'$ [a]

Method Basis	UHF [b] 6-31G*	GVB [c] 6-31G*	CCSD(T) 6-31G**	CCSD(T) DZP	CCSD(T) TZP	CCSD(T) C:PVTZ, H:DZP	CCSD(T) TZ2P
equilibrium geometry [d]							
$r_{C_1H_1}$	1.059	1.070	1.065	1.076	1.068	1.067	1.064
$r_{C_1C_2}$	1.317	1.322	1.310	1.324	1.310	1.296	1.304
$r_{C_2H_2}$	1.081	1.096	1.090	1.099	1.094	1.095	1.089
$r_{C_2H_3}$	1.081	1.096	1.090	1.099	1.094	1.095	1.089
$\angle H_2C_2C_1$	122.1	121.8	122.5	122.1	122.3	122.4	122.2
$\angle H_2C_2H_3$	115.8	116.4	115.0	115.9	115.3	115.2	115.5
rotational constants							
A			9.89064	9.63495	9.78676	9.78403	9.86067
B			1.03016	1.01095	1.03022	1.04743	1.03942
C			0.93298	0.91495	0.93210	0.94614	0.94030
fundamental vibrations							
ν_1	3583		3485	3426	3432	3416	3426
ν_2	3303		3160	3149	3119	3075	3122
ν_3	3240		3103	3080	3058	3025	3060
ν_4	1621		1657	1611	1628	1661	1626
ν_5	1434		1466	1431	1432	1419	1435
ν_6	1060		989	968	963	951	976
ν_7	960		932	895	926	932	930
ν_8	536		619	592	657	713	644
ν_9	917i		831i	806i	770i	744i	780i
energy	−77.37773		−77.67326	−77.70302	−77.73263	−77.76581	−77.75625
zero-point energy	22.50		22.030	21.663	21.750	21.717	21.756

[a] ACES II was used in the calculation. Bond lengths in Å, bond angles and diheral angles in deg, rotational constants in cm^{-1}, vibrational frequencies in cm^{-1}, energy in au and zero-point energy in kcal/mol.
[b] Ref. [8].
[c] Ref. [13].
[d] The atomic labeling is shown in Fig. 3 except that the H_1 is along the line with $C_1 = C_2$.

Table 8
The calculated barrier height for the rocking motion of α-H in C_2H_3 $\tilde{X}^2A'$

Method Basis	Exp. [a]	GVB [b] 6-31G**	MP4 [c] 6-31G**	CCSD(T) 6-31G**	CCSD(T) DZP	CCSD(T) TZP	CCSD(T) C:PVTZ, H:DZP	CCSD(T) TZ2P
classical (au)				−77.68323	−77.71302	−77.74103	−77.77343	−77.76493
transition state (au)				−77.67326	−77.70302	−77.73263	−77.76581	−77.75625
energy difference [d] (cm^{-1})	< 1500	3113	2168 (1539)	2188 (1683)	2195 (2029)	1844 (1396)	1672 (1241)	1905 (1477)

[a] Ref. [14].
[b] Ref. [13].
[c] Ref. [8].
[d] The number in parentheses represents the zero-point energy corrections for both classical and transition state of C_2H_3.

Table 9
The optimized geometry and energy difference of the isomeric C_2H_2 [a]

	Acetylene (H_2–C_2≡C_1–H_1)			Vinylidene (H_1,H_2>C_2=C_1)		
	exp. [b]	calc.		exp. [c]	calc.	
		Ref. [26] [c]	this work [d]		Ref. [26] [c]	this work [d]
$r_{C_1C_2}$	1.2026	1.2017	1.2081		1.3008	1.3050
$r_{C_2H_1}$					1.0818	1.0840
$r_{C_1H_1}$	1.0622	1.0616	1.0634			
$r_{C_2H_2}$	1.0622	1.0616	1.0634		1.0818	1.0840
$\angle C_1C_2H_1$					120.13	120.22
$\angle H_1C_2H_2$					119.74	119.56
$\angle C_2C_1H_1$		180	180			
$\angle C_1C_2H_2$		180	180			
energy (au)		−77.18537	−77.20065		−77.11765	−77.13087
energy difference (kcal/mol)		0	0	46.4 ± 5.5	42.39	43.76

[a] Bond lengths in Å, bond angles in deg.
[b] From Ref. [25].
[c] CCSD/TZ2P was used in the calculation.
[d] CCSD(T)/TZ2P is used in the calculation.
[e] From Ref. [27].

MBPT and CCSD(T), we have restricted the non-classical C_2H_3 to be of C_2 symmetry with five internal co-ordinates in the optimization. The optimized structures from various methods and basis sets are tabulated in Table 5, in which the computed fundamental vibrational frequencies of the non-classical C_2H_3 are also listed. In the CCSD(T) calculations for the vibrations of the non-classical C_2H_3, an imaginary vibrational frequency was always found, thus indicating the non-classical structure as an unstable isomer corresponding to a transition state on the molecular potential energy hypersurface. Comparisons for the calculated energy difference between the non-classical and the classical isomers of C_2H_3 are listed in Table 6.

2.2.2. α-H rocking motion

In a recent observation of the ν_7 vibrational band in C_2H_3 $\tilde{X}\,^2A'$, Kanamori et al. [14] have reported that the α-hydrogen (H_1 in Fig. 3) of C_2H_3 is rocking back and forth around the two equivalent sp^2 positions of the C_1 atom, corresponding to a tunnelling motion in a double-minimum potential. In this study, we have tried to accurately calculate the barrier of the rocking motion by using the ACES II program. We have optimized the *planar* transition state (**2** in Fig. 1) and calculated its fundamental vibrational frequencies. The results are listed in Table 7 with the similar atomic labelling as in Fig. 3 except that H_1 is along $C_1 = C_2$. The energy comparison between the transition state and the classical structure of C_2H_3 (**1** in Fig. 1), which is located in the global minimum of the potential energy hypersurface, is shown in Table 8.

2.3. Dissociation of C_2H_3 $\tilde{X}\,^2A'$

In calculating the dissociation of C_2H_3 $\tilde{X}\,^2A'$, the decomposition channels to acetylene and to vinylidene have been considered. The CCSD(T) method and TZ2P basis set were used in the calculation with the ACES II program. The dissociation energies for $C_2H_3 \rightarrow HCCH + H$ and $C_2H_3 \rightarrow H_2CC + H$ are calculated to be 40.70 and 84.46 kcal/mol, respectively. The optimized geometries of acetylene and vinylidene and the energy difference between these two isomers are listed in Table 9.

3. Discussion

3.1. Molecular structure

3.1.1. Equilibrium geometry and vibrations of C_2H_3 $\tilde{X}\,^2A'$

Comparing the experimental values, the optimized geometry for the classical structure of C_2H_3 $\tilde{X}\,^2A'$

(in Table 1) has shown a better accuracy for the CCSD(T) method than for MP2 and MP4. The use of 6-31G** in the CCSD(T) calculation seems to have a fairly good result in this case. While the structure calculated from Dunning's DZP basis set turned out to be not quite satisfactory, the triple zeta polarizations have much improved the results, especially for $\angle C_2C_1H_1$. The calculated rotational constants (A, B, and C) using PVTZ/DZP or TZ2P in CCSD(T) are very close to the experimental values. Nevertheless, one should note that the observed geometry is for the vibrational ground state and may differ slightly from the calculated equilibrium structure. Moreover, the observed rotational constants are responsible for a geometry of C_{2v} effective symmetry in C_2H_3, while the calculated one is of C_S. The slightly larger rotational constant A in the observation, in comparison with the calculated one, is in line with reasoning the *linearity* along $H_1C_1C_2$ due to α-H tunnelling.

The fundamental vibrational frequencies of the classical C_2H_3 $\tilde{X}\,^2A'$ obtained from the calculation are also tabulated in Table 1. As mentioned before, ν_7 has the strongest infrared intensity, and is the only vibrational mode observed so far. In view of this ν_7 vibration, poor vibrational frequencies resulted from the calculations at levels of SCF and MP. The CCSD(T) calculations, on the other hand, have given quite satisfactory results for the ν_7 vibrational frequency, indicative of the substantial improvement for the potential energy hypersurface due to electron correlation.

3.1.2. Electronic energies, ionization potential and dipole moment

In comparison with the observed vertical transition energies of C_2H_3 $\tilde{A}\,^2A'' \leftarrow \tilde{X}\,^2A'$ (24815 cm^{-1}) and of the ionization potential (8.25 eV), the calculated values (in Table 3) have gradually approached the experimental results from the uses of RASSCF to MRCI. The calculated 25529 cm^{-1} for $\tilde{A}\,^2A'' \leftarrow \tilde{X}\,^2A'$ and 8.33 eV for the ionization potential from the MRCI method are in excellent agreement with the observations. The small deviations between the calculated and the experimental values, i.e. only 714 cm^{-1} for $\tilde{A}\,^2A'' \leftarrow \tilde{X}\,^2A'$ and 80 meV for the ionization potential, have demonstrated a very good quality in the present computation. The vertical transition energy of 43910 cm^{-1} ($\sim$ 228 nm) for $\tilde{B}\,^2A' \leftarrow \tilde{X}\,^2A'$, obtained from the MRCI calculation, will be very helpful for us to experimentally search for the undiscovered $\tilde{B}\,^2A'$ state of C_2H_3 by laser spectroscopy. The transition moment of $\tilde{B}\,^2A' \leftarrow \tilde{X}\,^2A'$ should be substantial for spectroscopic observation due to its $\pi^* \leftarrow \pi$ character. The bond orders between the C–C of C_2H_3 for the $\tilde{X}$, $\tilde{A}$ and $\tilde{B}$ electronic states are 2, $1\frac{1}{2}$ and 1, respectively. The bond-order calculation is indeed reconciled with the long vibrational progression, due to the C–C stretch mode, observed in C_2H_3 $\tilde{A}\,^2A'' \leftarrow \tilde{X}\,^2A'$ [7]. The permanent dipole moment in C_2H_3 $\tilde{X}\,^2A'$ obtained from this work is also in good agreement with the previous generalized valence bond wavefunction calculation [13].

3.2. Intramolecular rearrangement

3.2.1. Isomerization

The optimized geometry, rotational constants and vibrational frequencies of the non-classical C_2H_3 $\tilde{X}\,^2A'$ are listed in Table 5. The shortening of the C–C bond-length in the non-classical C_2H_3 $\tilde{X}\,^2A'$, in comparison with that of the classical structure, is caused by the bridging hydrogen, H_1, the presence of which results in a doubly occupied orbital which resembles a C–C π-bonding orbital. In all of the CCSD(T) calculations, the imaginary vibrational frequency around 2100 cm^{-1} has indicated the very unstable nature of the non-classical isomeric structure. In Table 6, the energy difference between the classical and non-classical structures of C_2H_3 is represented. Including zero-point energy, the non-classical isomer has been found to lie at least 47 kcal/mol above the classical, and energetically far above the dissociation threshold (40.70 kcal/mol) of $C_2H_3 \rightarrow HCCH + H$. The large energy difference between the two isomers and the unstable nature of the non-classical structure have made the isomerization process in C_2H_3 quite a challenge for spectroscopic observation.

3.2.2. α-H rocking motion

In the determination of the barrier height for α-H tunnelling in C_2H_3 $\tilde{X}\,^2A'$, we have optimized the transition state (**2** in Fig. 1) as listed in Table 7. The vibrational frequencies associated with the transition state have accordingly shown an imaginary value

responsible for this saddle-point on the potential energy hypersurface. The calculated barrier height for the rocking motion of α-H in C_2H_3 $\tilde{X}\,^2A'$ is tabulated in Table 8. The barriers with zero-point energy correction, computed from CCSD(T)/Dunning's triple zeta polarizations, are in excellent agreement with the upper bound limit of < 1500 cm^{-1} determined by high-resolution infrared spectroscopy [14].

3.3. Dissociation of C_2H_3 $\tilde{X}\,^2A'$

In comparison with the experimental values of 80.0 ± 5.0 kcal/mol for the dissociation of $C_2H_3 \rightarrow H_2CC + H$ reported by Ervin et al. [27], the calculated 84.46 kcal/mol is in agreement with the measurement. The calculated energy difference of 43.76 kcal/mol between the isomers of acetylene and vinylidene is also consistent with the spectroscopic determination of 46.4 ± 5.5 kcal/mol [27].

4. Conclusion

We have carried out a systematic study of the molecular structure (including equilibrium geometry, vibrational frequencies and intensities, electronic energies, ionization potential and dipole moment), the intramolecular rearrangement (isomerization and α-H rocking motion) and the dissociation of C_2H_3 with high-level ab initio calculations using ACES II and MOLCAS-2 programs. In view of the calculated and the experimental values, such as the equilibrium geometry of C_2H_3 $\tilde{X}\,^2A'$, the transition energy of $\tilde{A}\,^2A'' \leftarrow \tilde{X}\,^2A'$, the ionization potential, the barrier height for the α-H rocking motion and the C–H dissociation energy, the computational accuracy in the present study has demonstrated to be of very good quality.

The vertical electronic transition $\tilde{B}\,^2A' \leftarrow \tilde{X}\,^2A'$ of C_2H_3 and the energy difference between the classical and non-classical isomers in C_2H_3 $\tilde{X}\,^2A'$, resulted from the calculations in this work, have provided valuable information which will facilitate the forthcoming experimental studies in our laboratory. The calculated vibrational frequencies and infrared intensities of C_2H_3 $\tilde{X}\,^2A'$ will assist the spectroscopic measurement for the unobserved vibrational modes. The knowledge from the calculated isomerization and dissociation processes in C_2H_3 $\tilde{X}\,^2A'$ will help us in the experimental investigations to be carried out with high-resolution IR-UV laser-induced grating spectroscopy.

Acknowledgement

We thank Professor S.H. Lin and Dr. J.-W. Yu for their comments on this manuscript. Mr. Chung-Jen Wu is gratefully acknowledged for his computer drawing of Fig. 4. This work is supported, in part, by the National Science Council of Republic of China under grant No. NSC-84-2113-M-001-037 CT.

References

[1] H. Okabe, Photochemistry of small molecules (Wiley, New York, 1978).
[2] W.C. Gardiner, Jr., ed., Combustion chemistry (Springer, New York, 1984).
[3] I.K. Puri, ed., Environmental implications of combustion processes (CRC Press, Boca Raton, 1993).
[4] A. Fahr, A. Laufer, R. Klein and W. Braun, J. Phys. Chem. 95 (1991) 3218.
[5] D.J. Donaldson, I.V. Okuda and J.J. Sloan, Chem. Phys. 193 (1995) 37.
[6] O. Simamura, in: Topics in stereochemistry, Vol. 4, eds., E.L. Eliel and N.L. Allinger (Wiley, New York, 1969) p. 1.
[7] H.E. Hunziker, H. Kneppe, A.D. McLean, P. Siegbahn and H.R. Wendt, Can. J. Chem. 61 (1983) 993.
[8] M.N. Paddon-Row and J.A. Pople, J. Phys. Chem. 89 (1985) 2768.
[9] L.A. Curtiss and J.A. Pople, J. Chem. Phys. 88 (1988) 7405.
[10] F.P. Lossing, Can. J. Chem. 49 (1971) 357.
[11] J. Berkowiz, C.A. Mayhew and B. Ruscic, J. Chem. Phys. 88 (1988) 7396.
[12] J.A. Blush and P. Chen, J. Phys. Chem. 96 (1992) 4138.
[13] M. Dupuis and J.J. Wendoloski, J. Chem. Phys. 80 (1984) 5696.
[14] H. Kanamori, Y. Endo and E. Hirota, J. Chem. Phys. 92 (1990) 197.
[15] R.A. Shepherd, T.J. Doyle and W.R.M. Graham, J. Chem. Phys. 89 (1988) 2738.
[16] M.W. Crofton, M.F. Jagod, B.D. Rehfuss and T. Oka, J. Chem. Phys. 91 (1989) 5139, and references therein.
[17] C. Liang, T.P. Hamilton and H.F. Schaefer III, J. Chem. Phys. 92 (1990) 3653, and references therein.
[18] L.B. Harding, J. Am. Chem. Soc. 103 (1981) 7469.
[19] I.M.B. Nielsen, C.L. Janssen, N.A. Burton and H.F. Schaefer III, J. Phys. Chem. 96 (1992) 2490.

[20] C.E. Hamilton, J.L. Kinsey and R.W. Field, Annu. Rev. Phys. Chem. 37 (1986) 493.
[21] M.A. Buntine, D.W. Chandler and C.C. Hayden, J. Chem. Phys. 97 (1992) 707.
[22] ACES II is authored by J.F. Stanton, J. Gauss, J.D. Watts, W.J. Lauderdale and R.J. Bartlett., University of Florida, USA.
[23] MOLCAS is authored by K. Andersson, M.P. Fülscher, G. Karlstrom, R. Lindh, P.-A. Malmqvist, J. Olsen B.O. Roos and A.J. Sadlej, University of Lund, Sweden.
[24] J. Almlöf and P.R. Taylor, J. Chem. Phys. 86 (1987) 4070.
[25] G. Strey and I.M. Mills, J. Mol. Spectry. 59 (1976) 103.
[26] J.F. Stanton, C.-M. Huang and P.G. Szalay, J. Chem. Phys. 101 (1994) 356.
[27] K.M. Ervin, J. Ho and W.C. Lineberger, J. Chem. Phys. 91 (1989) 5974.